Modulation of Kv4.2/KChIP3 interaction by the ceroid lipofuscinosis neuronal 3 protein CLN3

Received for publication, April 10, 2020, and in revised form, June 22, 2020 Published, Papers in Press, July 7, 2020, DOI 10.1074/jbc.RA120.013828

Carolin Seifert[1], **Stephan Storch**[2], **and Robert Bähring**[1,*]

From the [1]*Institut für Zelluläre und Integrative Physiologie, Zentrum für Experimentelle Medizin and the* [2]*Klinik und Poliklinik für Kinder- und Jugendmedizin, Pädiatrische Forschung, Universitätsklinikum Hamburg-Eppendorf, Hamburg, Germany*

Edited by Mike Shipston

Voltage-gated potassium (Kv) channels of the Kv4 subfamily associate with Kv channel–interacting proteins (KChIPs), which leads to enhanced surface expression and shapes the inactivation gating of these channels. KChIP3 has been reported to also interact with the late endosomal/lysosomal membrane glycoprotein CLN3 (ceroid lipofuscinosis neuronal 3), which is modified because of gene mutation in juvenile neuronal ceroid lipofuscinosis (JNCL). The present study was undertaken to find out whether and how CLN3, by its interaction with KChIP3, may indirectly modulate Kv4.2 channel expression and function. To this end, we expressed KChIP3 and CLN3, either individually or simultaneously, together with Kv4.2 in HEK 293 cells. We performed co-immunoprecipitation experiments and found a lower amount of KChIP3 bound to Kv4.2 in the presence of CLN3. In whole-cell patch-clamp experiments, we examined the effects of CLN3 co-expression on the KChIP3-mediated modulation of Kv4.2 channels. Simultaneous co-expression of CLN3 and KChIP3 with Kv4.2 resulted in a suppression of the typical KChIP3-mediated modulation; *i.e.* we observed less increase in current density, less slowing of macroscopic current decay, less acceleration of recovery from inactivation, and a less positively shifted voltage dependence of steady-state inactivation. The suppression of the KChIP3-mediated modulation of Kv4.2 channels was weaker for the JNCL-related missense mutant $CLN3_{R334C}$ and for a JNCL-related C-terminal deletion mutant (CLN3ΔC). Our data support the notion that CLN3 is involved in Kv4.2/KChIP3 somatodendritic A-type channel formation, trafficking, and function, a feature that may be lost in JNCL.

Voltage-gated potassium (Kv) channels are critically involved in the control of neuronal excitability and action potential waveform (1). Members of the Kv4 subfamily, especially Kv4.2, carry a subthreshold-activating somatodendritic A-type current (I_{SA}) (2), which mediates synaptic filtering and controls the spread of dendritic excitation (3, 4). Notably, Kv4.2 channel-mediated I_{SA} is down-regulated in animal models of cortical malformations and epilepsy (5–11).

Kv4 channels may form ternary complexes with auxiliary Kv channel–interacting proteins (KChIPs) (12) and dipeptidyl-aminopeptidase-related proteins (DPPs) (13). In heterologous expression systems, both auxiliary subunits cause an increase in Kv4 channel surface expression (12–16). Moreover, KChIPs and DPPs modulate Kv4 channel gating in a specific manner: KChIPs cause a slowing of macroscopic current decay and a positive shift in the voltage dependence of steady-state inactivation (12, 14, 15, 17), whereas DPPs cause an acceleration of macroscopic current decay and a negative shift of the voltage dependence of both activation and steady-state inactivation (13, 16, 18). Both auxiliary subunits cause an acceleration of recovery from inactivation (12–18). Among the four different known KChIP subtypes (19), KChIP3 seems to be special, because it is known to interact not only with Kv4 channels but also with DNA to act as a transcription repressor (KChIP3 is then usually referred to as DREAM, for downstream regulatory element antagonist modulator) (20). Moreover, KChIP3 may interact with the Ca^{2+}-signaling protein presenilin (KChIP3 is then usually referred to as calsenilin) (Ref. 21; reviewed in Ref. 22). More recently, it has been reported that KChIP3 (calsenilin, DREAM) may also interact with the late endosomal/lysosomal membrane glycoprotein ceroid lipofuscinosis neuronal 3 (CLN3; Fig. S1) (23). The functional role of CLN3 is still poorly defined, but numerous loss-of-function mutations in the *CLN3* gene are associated with juvenile neuronal ceroid lipofuscinosis (JNCL), an autosomal recessively inherited lysosomal storage disorder often referred to as juvenile CLN3 disease (24–26). JNCL is a childhood-onset neurodegenerative disease with first symptoms starting at the age of 4–8 years. More than 70 mutations have been identified in the *CLN3* gene with a genomic 1.02-kb deletion most frequently found (~85%) in JNCL patients (Fig. S1) (24). Here we asked whether CLN3, by its interaction with KChIP3 (23), may indirectly influence Kv4.2 channel surface expression and/or inactivation gating and whether these effects may differ for WT CLN3 and JNCL-related CLN3 mutants. The results of our experiments support the intriguing notion that the Kv4.2/KChIP3 somatodendritic A-type channel formation, trafficking, and function involve CLN3. This involvement may be reduced or completely lost in JNCL.

Results

CLN3 impairs Kv4.2/KChIP3 complex formation

It has been reported previously that CLN3 can bind to KChIP3 (23). Therefore, we asked whether co-expression of CLN3 may influence the binding of KChIP3 to the Kv4.2 channel protein. For this purpose, we expressed the epitope-tagged versions of Kv4.2, KChIP3, and CLN3, as well as untagged CLN3 in human embryonic kidney (HEK) 293 cells (see

This article contains supporting information.

* For correspondence: Robert Bähring, r.baehring@uke.de.

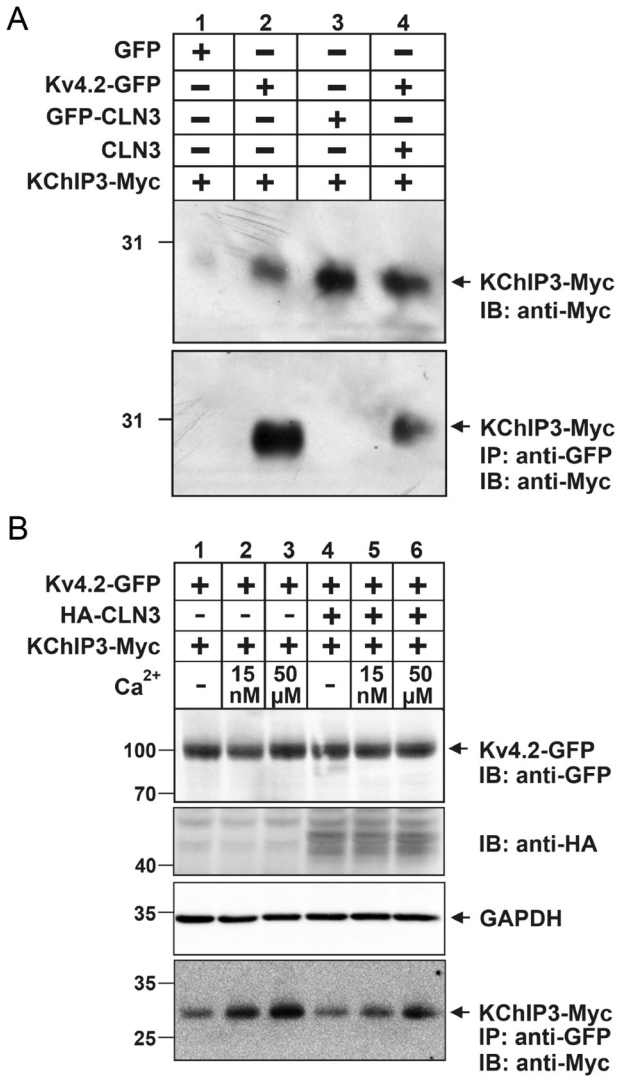

Figure 1. CLN3 and Ca^{2+} can influence Kv4.2/KChIP3 binding. For co-IP experiments HEK 293 cells were transiently transfected with Kv4.2–GFP and KChIP3–Myc in the absence or presence of CLN3, GFP–CLN3, or HA–CLN3 (see "Experimental procedures"). *A*, co-expression of Kv4.2–GFP and KChIP3–Myc in the absence (*lane 2*) or presence (*lane 4*) of CLN3. GFP co-transfected with KChIP3–Myc (*lane 1*) and GFP–CLN3 co-transfected with KChIP3–Myc (*lane 3*) were used as negative and positive input controls, respectively. 10% of the input fractions (*lanes 1–4*) were separated by SDS-PAGE and analyzed by Myc immunoblotting (*IB*; see "Experimental procedures"). Note the prominent signal in the absence (*lane 2*) and the weaker signal in the presence of CLN3 (*lane 4*). Surprisingly, KChIP3–Myc could not be precipitated from extracts of cells co-expressing GFP–CLN3 and KChIP3–Myc in the absence of Kv4.2–GFP. *B*, HEK 293 cells were co-transfected with Kv4.2–GFP, KChIP3–Myc, and either empty pcDNA3.1 vector or HA–CLN3. The lysis, co-precipitation, and washing steps were performed in nominal Ca^{2+}-free buffers (−) or in the presence of different Ca^{2+} concentrations (15 nM and 50 μM; see "Experimental procedures"). Prior to co-IP analyses, aliquots of the input fractions were probed with antibodies against GFP and HA. Equal loading was confirmed by glyceraldehyde-3-phosphate dehydrogenase (*GAPDH*) immunoblotting. After immunoprecipitation of Kv4.2–GFP, bound KChIP3–Myc was detected by Myc immunoblotting. Co-IP of Kv4.2–GFP and KChIP3–Myc was tested in the absence (*lanes 1–3*) and presence of HA–CLN3 (*lanes 4–6*) and with different Ca^{2+} concentrations in the lysis and washing buffers. *Lanes 1* and *4*, nominal Ca^{2+}-free (−); *lanes 2* and *5*, 15 nM Ca^{2+}; *lanes 3* and *6*, 50 μM Ca^{2+}. Note the stronger signals in higher Ca^{2+} both in the absence and in the presence of HA–CLN3. The positions of molecular weight markers are indicated. The results shown in *A* and *B* were confirmed in three independent experiments.

"Experimental procedures"). Extracts from cells co-expressing Kv4.2–GFP and KChIP3–Myc in the absence or presence of GFP–CLN3 (or untagged CLN3) were prepared, and Kv4.2–GFP was precipitated using GFP–TRAP beads (Fig. 1*A*; see "Experimental procedures"). Analyses of bound proteins showed that Kv4.2–GFP, but not GFP alone, precipitated KChIP3–Myc (Fig. 1*A*, *lanes 1* and *2*), confirming the direct interaction between Kv4.2 and KChIP3. Unexpectedly, we obtained no co-immunoprecipitation (co-IP) signal for GFP–CLN3 + KChIP3–Myc (Fig. 1*A*, *lane 3*; see "Discussion"); however, in extracts from cells expressing Kv4.2–GFP + KChIP3–Myc in the presence of CLN3, the amount of precipitated KChIP3–Myc was strongly reduced compared with extracts from cells expressing Kv4.2–GFP + KChIP3–Myc in the absence of CLN3 (Fig. 1*A*, *lanes 2* and *4*; see also Fig. S2). These results, which were confirmed in three independent experiments, support the notion that the molecular interaction between Kv4.2 and KChIP3 is impaired in the presence of CLN3. Because the KChIP3/CLN3 interaction has been reported to be weaker in high Ca^{2+} (23), we performed co-IP experiments with either 0 nM (nominal Ca^{2+}-free), 15 nM or 50 μM Ca^{2+} in the lysis, co-IP, and wash buffer (Fig. 1*B*; see "Experimental procedures"). Co-IP analyses of extracts from cells expressing Kv4.2–GFP + KChIP3–Myc showed higher amounts of precipitated KChIP3–Myc with increasing Ca^{2+} concentrations, both in the absence (Fig. 1*B*, *lanes 1–3*) and in the presence of hemagglutinin (HA)–CLN3 (Fig. 1*B*, *lanes 4–6*). For all tested Ca^{2+} concentrations, the amount of precipitated KChIP3–Myc was lower in the presence of HA–CLN3 compared with extracts expressing Kv4.2–GFP + KChIP3–Myc in the absence of HA–CLN3 (Fig. 1*B*; see also Fig. S2). The results of three such experiments confirmed the impairment of Kv4.2/KChIP3 binding by CLN3, even in high Ca^{2+}. Notably, our data also suggest that Kv4.2/KChIP3 binding is *per se* Ca^{2+}-dependent.

CLN3 suppresses KChIP3-mediated modulation of Kv4.2 channels

Given the impairment of Kv4.2/KChIP3 binding by CLN3, we tested whether CLN3 may interfere with the typical KChIP3-mediated modulation of Kv4.2 channels. For this purpose we performed whole-cell patch-clamp experiments on transfected HEK 293 cells (see "Experimental procedures"). Kv4.2-mediated currents were recorded on the first (d1) and on the second day (d2) after transfection (Fig. 2*A*). There was an increase in the current density mediated by homomeric Kv4.2 channels from 125 pA/pF on d1 (n = 7) to 216 pA/pF on d2 (n = 12), but co-expression of CLN3 had no effect on current density on either day (n = 9 and 12, respectively; Fig. 2*B*). KChIP3 co-expression, on the other hand, caused a strong increase in current density on both d1 and d2 (n = 15 and 9, respectively). If Kv4.2 was simultaneously co-expressed with KChIP3 and CLN3, the KChIP3-mediated increase in current density was strongly suppressed on d1 (n = 17) and virtually absent on d2 (n = 24; Fig. 2*B*; see also Table S1).

We asked whether the presence of CLN3 may also suppress the KChIP3-mediated modulation of the kinetics and voltage dependence of Kv4.2 channel inactivation and measured the

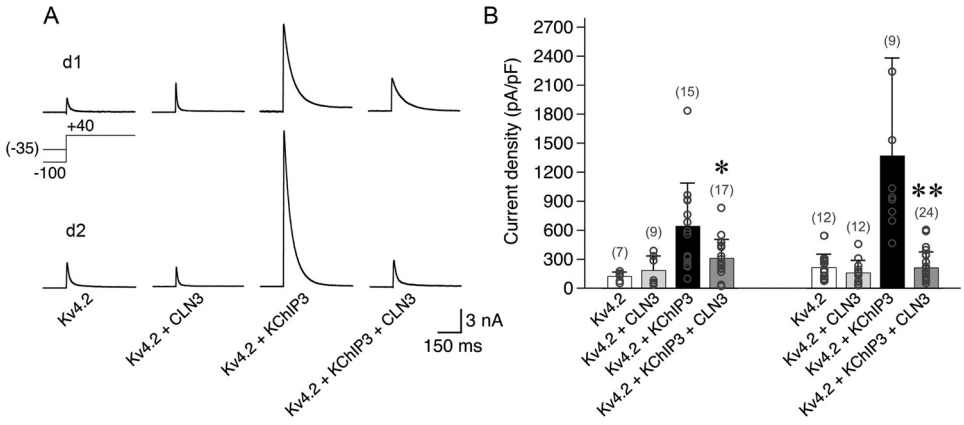

Figure 2. Effects of KChIP3 and CLN3 on Kv4.2-mediated current densities. For electrophysiological recordings, HEK 293 cells were transiently transfected with Kv4.2 or with Kv4.2 + KChIP3, each in the absence or presence of CLN3 (see "Experimental procedures"). *A*, currents were recorded on d1 and d2. Channels were activated by voltage jumps from −100 to +40 mV, and current traces were leak-subtracted with a −35 mV prepulse–inactivation–subtraction protocol (64). *B*, current densities were calculated based on the measured peak current amplitude and the corresponding whole-cell capacitance. The data are presented as means ± S.D., the number of observations (*n*) is indicated for each group, and individual data points are shown (*gray circles*). The typical increase in Kv4.2 current densities caused by KChIP3 co-expression is strongly attenuated in the presence of CLN3. Statistical analyses were done with one-way ANOVA and Dunnett's post hoc testing. *Asterisks* indicate values significantly different in the presence of CLN3 compared with Kv4.2 + KChIP3: *, $p < 0.05$; **, $p < 0.0001$ (see also Table S1).

relevant parameters on d2. Kv4.2-mediated currents showed a multiphasic decay, which was best described by the sum of three exponential functions (Fig. 3, *A* and *B*). The mean time constants obtained for homomeric Kv4.2 channels were 13, 58, and 1480 ms with relative amplitudes of 74, 22, and 4%, respectively (n = 12). Surprisingly, CLN3 co-expression caused the Kv4.2-mediated currents to decay faster (n = 12; see "Discussion"), whereas KChIP3 co-expression caused the well-known slowing of initial current decay (n = 9) (12, 14, 17). If Kv4.2 was simultaneously co-expressed with both KChIP3 and CLN3, the KChIP3-mediated slowing of initial current decay was attenuated (n = 22; Fig. 3, *A* and *B*; see also Table S1). Next we studied the recovery from inactivation. The recovery kinetics were described by a single-exponential function with a mean time constant of 400 ms for homomeric Kv4.2 channels (n = 11). The recovery kinetics were not influenced by CLN3 co-expression (n = 8), but KChIP3 co-expression caused the well-known acceleration of recovery kinetics (n = 6; Fig. 3, *C* and *D*) (12, 14, 17). If Kv4.2 was simultaneously co-expressed with KChIP3 and CLN3, the recovery kinetics were in some cases biphasic, resulting in fast and a slow recovery components. This may be explained by different channel populations in the plasma membrane: one with fast kinetics (modified by KChIP3) and one with slow kinetics (not modified by KChIP3). A weighted recovery time constant, which was calculated for all Kv4.2 + KChIP3 + CLN3–expressing cells studied (n = 15), lay closer to the time constant of the slow component (Fig. 3*D*; see also Table S2). This indicates that CLN3 attenuated the KChIP3-mediated acceleration of recovery kinetics. Finally, we studied the voltage dependence of steady-state inactivation (Fig. 4). Inactivation was half-maximal at −64 mV with a slope factor of 7 mV for homomeric Kv4.2 channels (n = 9). The voltage dependence of steady-state inactivation was not influenced by CLN3 co-expression (n = 5) but strongly shifted in the positive direction and steepened by KChIP3 co-expression (n = 6). If Kv4.2 was simultaneously co-expressed with both KChIP3 and CLN3, the positive shift and the steepening of the voltage dependence were attenuated (n = 13; Fig. 4; see also Table S2).

Taken together, these data support the notion that CLN3 interferes with functional Kv4.2/KChIP3 interaction. As a consequence the pronounced KChIP3-mediated augmentation of Kv4.2 current density was completely abolished in the presence of CLN3 (Fig. 2*B*; d2). The typical KChIP3-mediated modulation of Kv4.2 gating parameters, on the other hand, was left intact to some degree in the presence of CLN3 (see Figs. 3 and 4 and "Discussion"). Therefore, we examined the dose dependence of the CLN3 effects in a stable Kv4.2-expressing cell line (62), which was transiently transfected with different amounts of KChIP3 and CLN3 cDNA (see "Experimental procedures" and Fig. S3). In a steady background of Kv4.2 expression (mean current density of 167 pA/pF, n = 6, when transfected only with empty pcDNA3.1 vector) either KChIP3 alone or KChIP3 together with CLN3 were expressed. The cDNA amounts for the transient transfection of the stable cell line were chosen to yield a KChIP3:CLN3 cDNA mass ratio of either 1:10 or 1:20 (see "Experimental procedures"). The results of these experiments ($3 \leq n \leq 7$) confirmed our findings obtained with transient transfection of Kv4.2 and indicated a dose dependence of the CLN3 effect on the functional Kv4.2/KChIP3 interaction. However, in the stable Kv4.2-expressing cell line, none of the CLN3 effects on the KChIP3-mediated channel modulation observed with a 1:10 ratio proved to be significant, and a 1:20 ratio significance was only reached for current density, for amp1 and amp2 of the macroscopic current decay kinetics, and for the voltage dependence of steady-state inactivation (Fig. S2 and Tables S1 and S2).

The CLN3 effect on functional Kv4.2/KChIP3 interaction is Ca^{2+}-dependent

Based on our finding that the Kv4.2/KChIP3 complex is stabilized by Ca^{2+} both in the absence and in the presence of CLN3 (Fig. 1*B*), we conducted whole-cell patch-clamp experiments with different amounts of free Ca^{2+} (nominal Ca^{2+}-free,

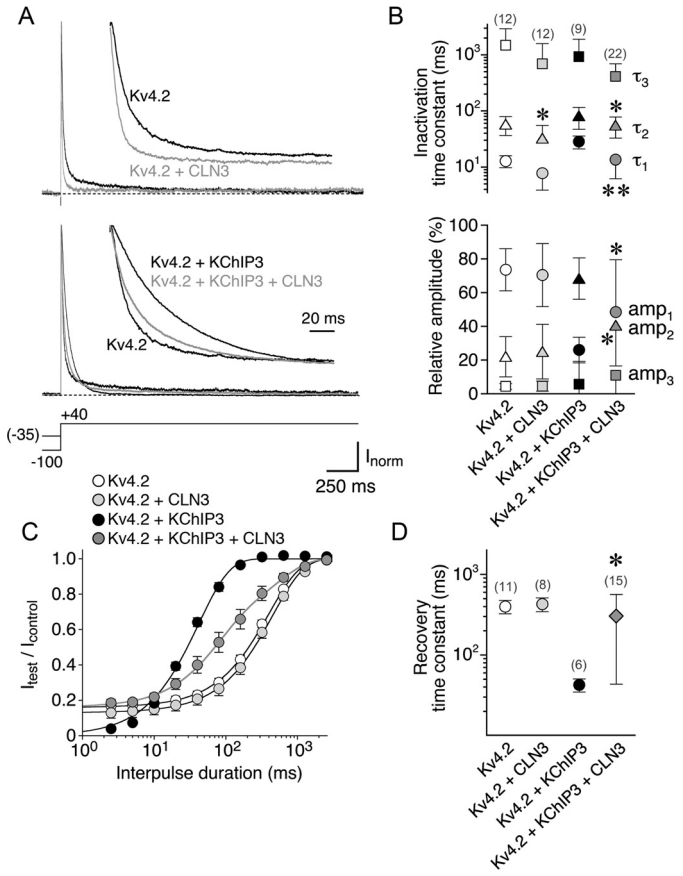

Figure 3. Effect of KChIP3 and CLN3 on Kv4.2 inactivation kinetics. *A*, currents mediated by Kv4.2 and Kv4.2/KChIP3 in the absence (*black traces*) or presence of CLN3 (*gray traces*). Current traces were leak-subtracted and normalized to peak. *Insets*, initial current decay kinetics shown on an expanded time scale. Note that CLN3 accelerated the decay kinetics of Kv4.2-mediated currents in the absence of KChIP3 (*upper traces*). The cross-over of normalized current traces, typically caused by KChIP co-expression, is still seen in the presence of CLN3, but the KChIP3-mediated slowing of the initial current decay is strongly attenuated by CLN3 (*lower traces*; the Kv4.2 trace in the absence of KChIP3 and CLN3 is shown as a reference). *B*, time constants of current decay (τ_1, τ_2, and τ_3) and their relative amplitudes (amp_1, amp_2, and amp_3 in %) obtained by triple-exponential fitting of the macroscopic current decays. *C*, the kinetics of recovery from inactivation were obtained by plotting relative current amplitudes ($I_{test}/I_{control}$, no leak subtraction) against the interpulse duration and fitting the data with a single-exponential or, if necessary, with a double-exponential function. *D*, recovery time constants obtained from single-exponential fitting (*circles*) and weighted time constant based on double-exponential fitting (*diamond*). The data in *B* and *D* are presented as means ± S.D., and the number of observations (*n*) is indicated for each group; the data in *C* are presented as means ± S.E. Statistical analyses were done with one-way ANOVA and Dunnett's post hoc testing. *Asterisks* indicate values significantly different in the presence of CLN3 compared with Kv4.2 alone or Kv4.2 + KChIP3. *, $p < 0.05$; **, $p < 0.0001$ (see also Tables S1 and S2).

15 nM Ca^{2+}, and 50 μM Ca^{2+}) in the pipette solution to manipulate in a controlled manner the cytoplasmic Ca^{2+} concentration (see "Experimental procedures"). The relevant electrophysiological parameters were measured on d2 for Kv4.2/KChIP3 channel complexes in the absence and in the presence of CLN3, and the data obtained with 15 nM Ca^{2+} ($n \leq 9$ and $n \leq 24$, respectively) in the patch-pipette served as control (Fig. 5). We first tested the Ca^{2+} dependence of Kv4.2/KChIP3 channels in the absence of CLN3 and found no significant differences for the well-known KChIP3-mediated modulation if Ca^{2+} was increased to 50 μM ($n \leq 14$). However, the KChIP3-mediated modulation in the absence of CLN3 was less pronounced in recordings with a nominal Ca^{2+}-free solution in the patch-pipette ($n \leq 20$), especially for the recovery kinetics and the voltage dependence of steady-state inactivation (Fig. 5, *D* and *E*). Intriguingly, for Kv4.2 + KChIP3 + CLN3, we observed a weaker CLN3 effect on the KChIP3-mediated channel modulation in 50 μM Ca^{2+} ($n \leq 14$; *i.e.* larger current density, slower current decay, faster recovery kinetics. and more positive voltage dependence of steady-state inactivation as compared with 15 nM Ca^{2+}; Fig. 5, *B–E*). For the inactivation kinetics (*i.e.* macroscopic current decay and recovery from inactivation; Fig. 5, *C* and *D*), but not for other parameters, the CLN3 effect on the KChIP3-mediated modulation was also weaker under nominal Ca^{2+}-free conditions ($n \leq 9$) as compared with 15 nM Ca^{2+}. The results of these experiments are summarized in Tables S3a and S3b. Taken together, the data suggest a Ca^{2+} dependence for both the KChIP3-mediated channel modulation *per se* and the CLN3-mediated attenuation of KChIP3-mediated channel modulation but apparently within different concentration ranges (see "Discussion").

JNCL-related CLN3 mutants exert weaker effects on functional Kv4.2/KChIP3 interaction

We tested two JNCL-related CLN3 mutants (the missense mutant $CLN3_{R334C}$ and the C-terminal deletion mutant CLN3ΔC; see Fig. S1 and "Experimental procedures") with our standard pipette solution (15 nM Ca^{2+}; Fig. 6). The relevant electrophysiological parameters were measured on d2 for Kv4.2 + KChIP3 + CLN3 (WT, $n \leq 24$), Kv4.2 + KChIP3 + $CLN3_{R334C}$ ($n \leq 16$), and Kv4.2 + KChIP3 + CLN3ΔC ($n \leq 17$). We asked, first, whether the electrophysiological parameters obtained with the CLN3 mutants differ from the ones obtained with WT CLN3, and second, whether the functional Kv4.2/KChIP3 interaction is still significantly affected by the CLN3 mutants (*i.e.* whether the electrophysiological parameters significantly differ from the ones obtained with maximal KChIP3-mediated modulation in the absence of CLN3). There was a trend toward weaker effects on Kv4.2/KChIP3 current densities, which proved to be significant for CLN3ΔC; however, similar to WT CLN3, both mutants still significantly affected the KChIP3-mediated modulation of current densities (Fig. 6*B*). The effects on Kv4.2/KChIP3 inactivation kinetics (macroscopic onset and recovery) were significantly weaker than the CLN3 WT effects for both $CLN3_{R334C}$ and CLN3ΔC, and the data showed no significant differences from the ones obtained with maximal KChIP3-mediated modulation (Fig. 6, *C* and *D*). Intriguingly, the effects of the mutants on the voltage dependence of steady-state inactivation were not significantly different from CLN3 WT effects, and in all cases the data differed significantly from the ones obtained with maximal KChIP3-mediated modulation (Fig. 6*E*; see also Tables S1 and S2). Taken together, our experimental results showed that, except for the voltage dependence of steady-state inactivation, the effects on Kv4.2/KChIP3 functional interaction were less pronounced for the tested CLN3 mutants than for WT CLN3. For the current density data, a trend is seen suggesting that functional surface expression of Kv4.2/KChIP3 channels is still strongly

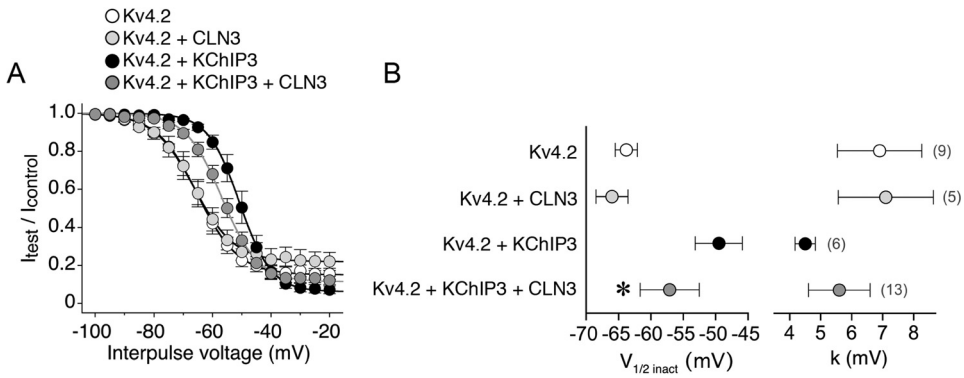

Figure 4. Effect of KChIP3 and CLN3 on the voltage dependence of Kv4.2 steady-state inactivation. *A*, relative current amplitudes (means ± S.E.) were plotted against the prepulse potential, and the data were fitted with a Boltzmann-function (see "Experimental procedures"). *B*, values obtained for the voltage of half-maximal inactivation ($V_{1/2\ inact}$) and the corresponding slope factor (*k*). The data are presented as means ± S.E. in *A* and as means ± S.D. in *B*, and the number of observations (*n*) is indicated for each group. Statistical analyses were done with one-way ANOVA and Dunnett's post hoc testing. *Asterisks* indicate values significantly different in the presence of CLN3 compared with Kv4.2 + KChIP3. *, $p < 0.05$ (see also Table S2).

suppressed by $CLN3_{R334C}$, similar to WT CLN3, whereas the suppression is moderate, albeit still significant, for CLN3ΔC.

Discussion

We tested whether CLN3, via its putative interaction with KChIP3, may influence Kv4.2/KChIP3 interaction and, thus, the expression level and inactivation gating of A-type potassium channels. The combined results of our co-IP and whole-cell patch-clamp experiments support this hypothesis and suggest that JNCL-related mutant CLN3 proteins have less influence on Kv4.2/KChIP3 interaction.

KChIP3 is a multifunctional neuronal calcium sensor involved in apoptosis

KChIPs belong to the neuronal calcium sensor (NCS) superfamily of Ca^{2+}-binding EF-hand proteins, and it was postulated that these auxiliary Kv4 channel β-subunits may regulate A-type currents and, thus, neuronal excitability in response to changes in cytoplasmic Ca^{2+} (12, 22). The data directly supporting this idea exist for cerebellar neurons, in which Kv4.2/KChIP3 complexes make a major contribution to I_{SA} (27). Ca^{2+} entering these cells through low voltage-activated Ca^{2+} channels is thought to bind to KChIP3, thereby promoting its modulatory functions including a positive shift in the voltage dependence of Kv4.2 channel steady-state inactivation. This guarantees a high I_{SA} availability at physiological membrane potentials (27). Our patch-clamp data obtained with Kv4.2/KChIP3 in the absence of CLN3 with a nominal Ca^{2+}-free and a 15 nM Ca^{2+} pipette solution, respectively, reflect this form of Ca^{2+}-dependent modulation of A-type potassium channels (Fig. 5, *D* and *E*). The observed Ca^{2+} effects on the KChIP3-mediated modulation of Kv4.2 channel gating may involve a stabilization of the Kv4.2/KChIP3 complex, as suggested by our co-IP data obtained in different Ca^{2+} concentrations (Figs. 2*B* and 6).

Before the identification of KChIPs as Kv4 channel β-subunits, proteins identical to KChIP3 had been identified in two different contexts as "DREAM" (a Ca^{2+}-dependent transcription repressor) (20) and "calsenilin" (a Ca^{2+}- and presenilin-binding protein) (21). KChIP3 (DREAM) binds to the downstream regulatory element of the prodynorphin gene (20), which relates KChIP3 to pain sensing. The other previously identified function relates KChIP3 (calsenilin) to intracellular Ca^{2+} homeostasis and brain pathophysiology, because mutations in the KChIP3-binding partner presenilin are associated with familial Alzheimer's disease (28). It is thought that, via its interaction with presenilin, KChIP3 controls other presenilin-binding partners (22). Because presenilin is tightly associated with endoplasmic reticulum (ER) Ca^{2+} release channels, KChIP3 is involved in the control of intracellular Ca^{2+} release (reviewed in Ref. 22). In fact, overexpression of KChIP3 modifies ER Ca^{2+} release and may lead to apoptosis (29, 30). Presenilin is also part of the γ-secretase enzyme complex, which mediates the γ-cleavage of amyloid precursor protein to produce Aβ peptides (reviewed in Ref. 22). Because of its interaction with presenilin, KChIP3 functions as a Ca^{2+} sensor for the γ-secretase, which mediates enhanced enzyme activity at elevated Ca^{2+} levels (31). The presenilin/γ-secretase enzyme complex is integral to the proapoptotic activity of KChIP3 (32).

The intriguing finding that KChIP3 can also interact with CLN3 (23) may add another aspect to the involvement of KChIP3 in brain pathophysiology, because mutated CLN3 is found in JNCL (24). On the other hand, it may shed more light on the hitherto not well-defined function of CLN3 (25). KChIP3 may represent a Ca^{2+} sensor for CLN3, similar to what is postulated for the other known KChIP3-binding partners. Chang *et al.* (23) found that the KChIP3/CLN3 interaction is disturbed in the presence of high Ca^{2+} (50 μM), possibly reflecting a regulatory mechanism similar to the Ca^{2+}-dependent dissociation of KChIP3 (DREAM) from DNA (20). Notably, KChIP3 and CLN3 seem to be opponents in the control of cell survival, because in contrast to KChIP3, CLN3 is anti-apoptotic. Overexpression of CLN3 suppresses Ca^{2+}-induced neuronal cell death, whereas down-regulation of CLN3 has the opposite effect, and additional down-regulation of KChIP3 in the same cells again prevents cell death (23). It is possible that the proapoptotic activity of KChIP3 can be neutralized by an interaction with CLN3. Moreover, KChIP3 has been reported to be up-regulated in CLN3 knockdown cells and in the brains of CLN3 knockout mice but down-regulated by CLN3 overexpression (23). From these data it has been concluded that CLN3 can negatively regulate cellular levels of KChIP3 expression.

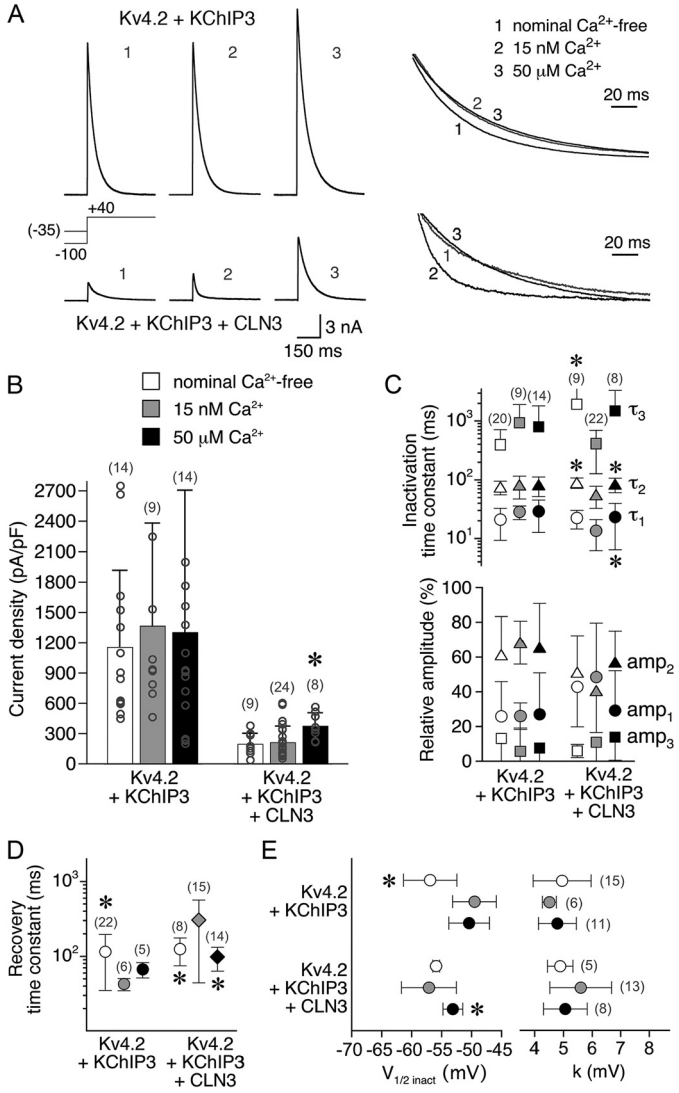

Figure 5. Ca^{2+} dependence of CLN3 effects on K4.2/KChIP3 functional interaction. Whole-cell patch-clamp experiments were performed with different free Ca^{2+} concentrations in the pipette solution (see "Experimental procedures"). *A*, currents recorded for Kv4.2 + KChIP3 (*upper row*) and Kv4.2 + KChIP3 + CLN3 (*lower row*) in nominal Ca^{2+}-free solution (*trace 1*), 15 nM Ca^{2+} (*trace 2*), and 50 μM Ca^{2+} (*trace 3*). *Insets* on the *right*, initial decays kinetics are shown on an expanded time scale (currents normalized to peak and superimposed). The functional parameters obtained for Kv4.2/KChIP3 channels in the absence and presence of CLN3 with nominal Ca^{2+}-free solution (*open symbols*), 15 nM Ca^{2+} (*gray symbols*), and 50 μM Ca^{2+} (*black* symbols) are shown. *B*, current densities. *C*, time constants of macroscopic current decay and their relative amplitudes. *D*, time constants of recovery from inactivation. *Diamonds* indicate weighted time constants. *E*, voltages of half-maximal inactivation ($V_{1/2\ inact}$) and corresponding slope factors (*k*). All data are presented as means ± S.D., the number of observations (*n*) is indicated for each group, and individual data points are shown in *B* (*gray circles*). Statistical analyses were done with one-way ANOVA and Dunnett's post hoc testing. *Asterisks* indicate values significantly different from the values obtained with 15 nM Ca^{2+}. *, $p < 0.05$ (see also Tables S3a and S3b).

Mode of CLN3 action on A-type potassium channels

The KChIP3/CLN3 interaction put forward by Chang *et al.* (23) represented the starting point for the present study. We hypothesized that, similar to the suppression of the proapoptotic activity of KChIP3, CLN3 may also suppress the KChIP3-mediated modulation of Kv4.2 channel surface expression, the KChIP3-mediated modulation of Kv4.2 channel inactivation gating, or both. Surprisingly, we found that CLN3 significantly accelerated the decay kinetics of Kv4.2-mediated currents even if KChIP3 was not co-expressed. Thus, CLN3 may either be able to directly interact with Kv4.2 channels, or it may activate other KChIP3-unrelated regulatory mechanisms, which influence Kv4.2 channel macroscopic inactivation. Although numerous CLN3 interaction partners have been identified (25), it is not known whether other KChIP or Kv4 isoforms interact with CLN3. This was not studied further because neither any of the other gating parameters examined nor current densities were influenced by CLN3 in the absence of exogenous KChIP3. On the other hand, we were able to show that CLN3 co-expression suppressed all aspects of the KChIP3-mediated Kv4.2 channel modulation. Thus, our experimental results fully confirm the formulated working hypothesis; however, they provide no direct information on the mode of CLN3 action. There are different not mutually exclusive possibilities: similar to the findings of Chang *et al.* (23), CLN3 may negatively regulate KChIP3 expression levels in HEK 293 cells. Although not systematically investigated, our Western blot data do not support this notion but rather suggest higher KChIP3–Myc levels in the presence of GFP-tagged and untagged CLN3 as compared with the KChIP3–Myc + GFP control (Fig. 1*A*). Higher KChIP3–Myc levels were also seen with Kv4.2–GFP co-expression. We think that both CLN3 (or GFP–CLN3) and Kv4.2–GFP co-expression exerted a stabilizing effect on KChIP3–Myc in our experiments. Such a stabilizing effect was indirectly shown by the finding that KChIP expression levels, especially KChIP3, are actually down-regulated in Kv4.2 and Kv4.3 knockout mice (33, 34).

Our combined results support the notion that CLN3, instead of decreasing exogenous KChIP3 expression levels, directly influences Kv4.2/KChIP3 complexes or their formation. The absence of a co-IP signal for KChIP3–Myc + GFP–CLN3 was unexpected and apparently contradicts the findings of Chang *et al.* (23). However, these authors used a glutathione *S*-transferase–KChIP3 fusion protein and untagged CLN3 instead of KChIP3–Myc and GFP–CLN3, respectively, as in our study. Because our data demonstrated undisturbed complex formation between KChIP3–Myc and Kv4.2–GFP (Fig. 1*A*), we suspect that the GFP tagging of CLN3 interfered with KChIP3–Myc association. On the other hand, our co-IP data clearly show that both untagged and HA-tagged CLN3 interfere with Kv4.2–GFP/KChIP3–Myc complex formation (Fig. 1*A* and Fig. S2).

CLN3 may compete with Kv4.2 for KChIP3 binding already during co-expression and co-trafficking (35) and withdraw KChIP3 from complex formation with Kv4.2. Alternatively, CLN3 may interact with mature Kv4.2/KChIP3 channel complexes in the plasma membrane to exert its effects. CLN3 is mainly located in the late endosomal/lysosomal compartment but has also been reported to reside, among others, in the ER, *trans*-Golgi network and plasma membrane (reviewed in Refs. 25 and 35). Given the numerous subcellular locations reported for CLN3 (35, 36), effects on immature Kv4.2/KChIP3 channels caused by co-expression and co-trafficking and effects on

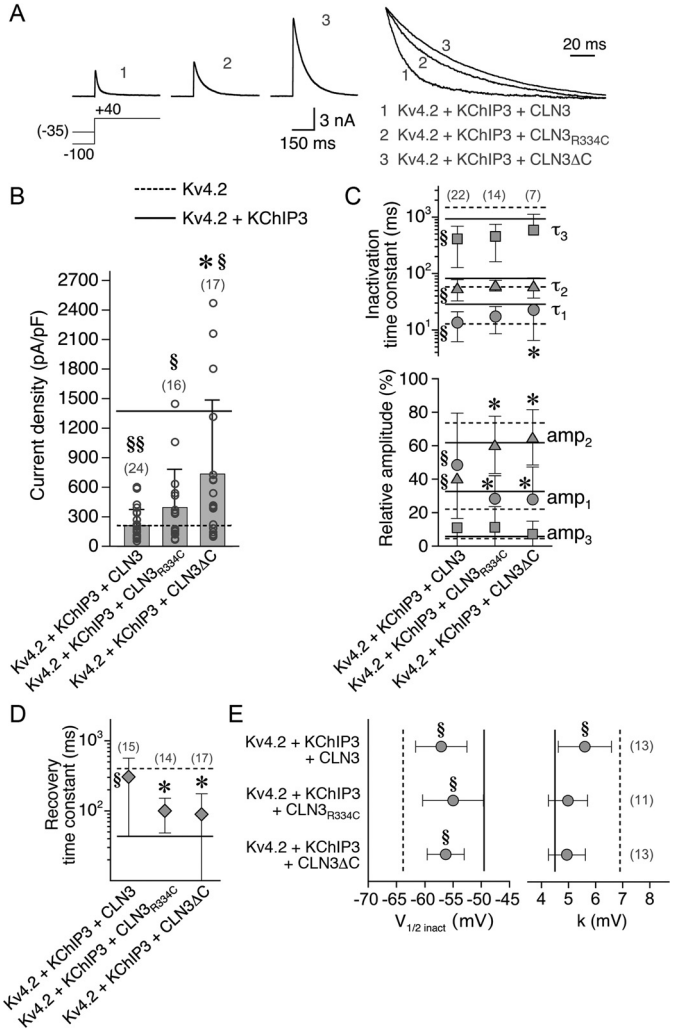

Figure 6. Effects of WT and mutant CLN3 on Kv4.2/KChIP3 functional interaction. Kv4.2/KChIP3 channels were co-expressed with WT and mutant CLN3 and functionally characterized. The missense mutant $CLN3_{R334C}$ and the C-terminal deletion mutant CLN3ΔC were tested. *A*, currents recorded for Kv4.2 + KChIP3 + CLN3 (WT, *trace 1*), Kv4.2 + KChIP3 + $CLN3_{R334C}$ (*trace 2*), and Kv4.2 + KChIP3 + CLN3ΔC (*trace 3*). *Inset* on the *right*, initial decay kinetics are shown on an expanded time scale (currents normalized to peak and superimposed). The functional parameters obtained for the three groups are shown. *B*, current densities. *C*, time constants of macroscopic current decay and their relative amplitudes. *D*, weighted time constants of recovery from inactivation. *E*, voltages of half-maximal inactivation ($V_{1/2\ inact}$) and corresponding slope factors (*k*). All data are presented as means ± S.D., the number of observations (*n*) is indicated for each group, and individual data points are shown in *B* (*gray circles*). *Horizontal* and *vertical broken lines*, mean values for Kv4.2 expressed alone (no KChIP3-mediated modulation); *horizontal* and *vertical solid lines*, mean values for Kv4.2/KChIP3 in the absence of CLN3 (maximal KChIP3-mediated modulation). Statistical analyses were done with one-way ANOVA and Dunnett's post hoc testing. *Asterisks* indicate values significantly different from Kv4.2/KChIP3 co-expressed with WT CLN3. *, $p < 0.05$. § symbols indicate a significant difference from the maximal KChIP3-mediated modulation. §, $p < 0.05$; §§, $p < 0.0001$ (see also Tables S1 and S2).

mature Kv4.2/KChIP3 channels in the plasma membrane are equally possible.

Our data suggest that CLN3 may disturb Kv4.2/KChIP3 complex formation, thereby negatively influencing the trafficking of Kv4.2 channels to the cell surface. It should be noted in this context that current density, which is a good correlate of channel surface expression, showed the highest CLN3 sensitivity. In fact, current density, unlike the other electrophysiological parameters examined, exhibited a complete neutralization of the KChIP3-mediated modulation when CLN3 was co-expressed (Fig. 2). Moreover, the moderate effects observed in the stable Kv4.2-expressing cell line (Fig. S3) support the idea that the CLN3 effects depend on co-expression and co-trafficking early in biogenesis.

Co-trafficking of CLN3 with Kv4.2 and KChIP3 to the cell periphery may render the KChIP3/CLN3 interaction Ca^{2+}-sensitive (35). The results obtained with glutathione *S*-transferase pulldown assays in 50 μM Ca^{2+} and with cells treated with the ER Ca^{2+} pump inhibitor thapsigargin have previously suggested that the KChIP3/CLN3 interaction is weaker in high Ca^{2+} (23). Thus, the negative influence of CLN3 on Kv4.2/KChIP3 interaction demonstrated by our own experiments should be relieved in high Ca^{2+}. Such an indirect Ca^{2+} dependence of the Kv4.2/KChIP3 interaction was probably masked in our co-IP experiments, which suggested that the Kv4.2–GFP/KChIP3–Myc interaction *per se* (*i.e.* in the absence of CLN3) was favored by Ca^{2+} (Fig. 1*B*). Aside from that, our quantified co-IP data suggest that even in the presence of 50 μM Ca^{2+}, HA–CLN3 co-expression still reduced Kv4.2–GFP/KChIP3–Myc interaction by 50% (Fig. S2). Only by performing whole-cell patch-clamp experiments with different Ca^{2+} concentrations in the pipette solution, we were able to resolve different modes of Ca^{2+}-dependent channel modulation. Our results suggest that increasing Ca^{2+} from 0 to 15 nM favors the KChIP3-mediated modulation of Kv4.2 channels, although this concentration lies below the hitherto reported *in vitro* K_d values for high affinity metal binding of KChIPs (10–50 μM) (22). On the other hand, differences between the current parameters measured with 15 nM and 50 μM Ca^{2+}, respectively, were only seen in the presence of CLN3 (Fig. 5). The latter results may be explained by a weakening of the KChIP3/CLN3 interaction in 50 μM Ca^{2+}, which favors the KChIP3-mediated modulation of Kv4.2 channels. Because all current parameters were measured within a time range between tens of seconds and a few minutes after establishing the whole-cell configuration, the observed Ca^{2+} effects can be classified as acute. Acute Ca^{2+} effects on the surface expression of Kv4.2/KChIP complexes in the whole-cell patch-clamp configuration have been studied previously by Murphy and Hoffman (37), who found increased Kv4.2 current densities with elevated Ca^{2+} in the pipette solution for certain KChIP isoforms including the KChIP3a splice variant used in the present study. The authors suggested a post-ER/Golgi pool of Kv4/KChIP channel complexes recruited to the plasma membrane in a Ca^{2+}-dependent manner. CLN3 may critically influence this short-distance surface membrane trafficking and, thus, the turnover of Kv4.2 channels in a KChIP3-dependent manner. It should be noted that CLN3 has been shown previously to be involved in the control of Na^+/K^+-ATPase turnover via the cytoskeletal protein fodrin (38). Taken together, CLN3 not only may influence Kv4.2/KChIP3 channel formation and trafficking early in biogenesis but may also play a role in the dynamic Ca^{2+}-dependent A-type channel trafficking and recycling at the plasma membrane.

CLN3 effects on Kv4.2/KChIP3 channels

A role for KChIP3 and somatodendritic A-type potassium channels in JNCL?

Knockout mice with targeted disruption of the *Cln3* gene ($Cln3^{-/-}$) and knockin mice, which harbor the most common alteration of the human *CLN3* gene ($Cln3^{\Delta ex7/8}$), have been created to be used as preclinical disease models for JNCL (39, 40). Both models exhibit the hallmarks of JNCL, including intracellular accumulation of autofluorescent storage material, astrocytosis, microglial activation, neuronal loss, and neurological deficits (39, 40). Given the typical neurological phenotype of JNCL, the previously shown interaction between the CLN3 protein and the Kv4 channel β-subunit KChIP3 (23) combined with the results of the present study leads to the question of whether KChIP3 and somatodendritic A-type potassium channels may play a role in JNCL.

A cellular hallmark of the neuronal ceroid lipofuscinoses (NCL) including JNCL is the accumulation of autofluorescent ceroid lipopigments with subunit c of mitochondrial ATP synthase or sphingolipid activator proteins A and D as major protein components (41). Autophagy, the process in which such intracellular macromolecules are normally digested during organelle turnover, requires the fusion of autophagic vacuoles with late endosomes and lysosomes. This process is disrupted in CLN3 deficiency leading to the accumulation of autophagic vacuoles accompanied by disturbed Ca^{2+} homeostasis (42, 43). The latter may represent an important mechanistic link between CLN3 and KChIP3 in JNCL, because the reported vulnerability of CLN3-deficient cells to Ca^{2+}-induced cytotoxicity following treatment with thapsigargin or with the Ca^{2+} ionophore A23187 is thought to be mediated by KChIP3 (23). CLN3 deficiency may lead to increased availability of KChIP3, which by its known interaction with presenilin may in an unphysiological manner influence ER Ca^{2+} channels (22, 30). Apparently, despite its important functions as a neuronal calcium sensor, too-high levels of free KChIP3 may be detrimental to cell function. In accordance with this notion, the down-regulation of KChIP expression levels observed in Kv4.2 knockout mice has been previously interpreted as a feedback mechanism to ensure that free KChIPs do not accumulate (33). Thus, a so-far-unconsidered role of CLN3, which is reduced or lost in JNCL, may be to keep cellular levels of free KChIP3 below a critical proapoptotic level at physiological and moderately increased cytoplasmic Ca^{2+} concentrations. A strong increase in cytoplasmic Ca^{2+} may augment the proapoptotic activity of KChIP3, a mechanism expected to be exaggerated by CLN3 loss of function as in JNCL. It should be noted that targeting KChIP3 with small molecule inhibitors has recently been considered a possible strategy for the treatment of Huntington's disease, which is another neurodegenerative disorder (44).

To find out whether JNCL-related mutant CLN3 proteins still affect Kv4.2/KChIP3 interaction, we tested the missense mutant $CLN3_{R334C}$ and the C-terminal deletion mutant CLN3ΔC, which is most common in JNCL (45) (Fig. S1). The effects of these mutants on the KChIP3-mediated modulation of Kv4.2 channels were weaker compared with WT CLN3, and concerning current density, the effect was weaker for CLN3ΔC than for $CLN3_{R334C}$ (Fig. 6*B*). The variable impact of the mutants on Kv4.2/KChIP3 interaction may be caused by their different protein stabilities, altered intracellular localization, and/or binding affinities for KChIP3. The missense mutation R334C does not impair lysosomal targeting of CLN3 but compromises its function (46), whereas the truncated CLN3ΔC protein is thought to be retained in the ER because of misfolding (47). It is likely that a large amount of mutant CLN3ΔC RNA is degraded (48); however, the observation that RNA interference–mediated down-regulation of residual CLN3ΔC-related transcripts had an effect on lysosomal size led to the conclusion that some residual function is still preserved in CLN3ΔC (49). The proposed residual function of CLN3ΔC may include a moderate effect on channel trafficking out of the ER. Notably, the CLN3ΔC mutant protein lacks the proposed binding site for KChIP3 encompassing C-terminal amino acids 314–438 (23) (Fig. S1) and is not expected to interact with KChIP3, unless additional as-yet-unidentified binding sites exist. The different degrees of suppression of the functional Kv4.2/KChIP3 interaction mediated by CLN3ΔC and $CLN3_{R334C}$, respectively, suggest that this effect is important only in JNCL patients with the CLN3ΔC deletion mutant but not in JNCL patients carrying the $CLN3_{R334C}$ mutation.

The results of our electrophysiological measurements obtained in the presence of WT and mutant CLN3 proteins support the notion that a physiological CLN3 effect on Kv4.2/KChIP3 interaction is reduced in JNCL. This in turn raises the question of whether and how the reduced regulatory effect on KChIP3-mediated channel modulation can be pathogenic. It should be noted in this respect that the $CLN3_{R334C}$ and CLN3ΔC-mediated Kv4.2/KChIP3 channel gain of function (compared with WT CLN3) observed in our experiments suggests increased I_{SA} availability caused by CLN3 loss of function in JNCL, a scenario in which somatodendritic excitability is expected to be reduced.

Because JNCL patients exhibit deficits in motor coordination and cerebellar atrophy (50–52), cerebellar neurons, especially cerebellar granule cells, have moved into the focus of preclinical JNCL research. In both $Cln3^{-/-}$ and $Cln3^{\Delta ex7/8}$ mice, cerebellar granule cells show a higher vulnerability to α-amino-3-hydroxy-5-methyl-4-isoxazolepropionic acid (AMPA) receptor-mediated excitotoxicity (53, 54). Altered AMPA receptor trafficking and enhanced AMPA receptor function have been initially suggested to underlie the increased AMPA receptor-mediated excitotoxicity in $Cln3^{-/-}$ mice (54). However, a more recent detailed examination of the physiology of the mossy fiber–granule cell synapse performed by Studniarczyk *et al.* (55) found no differences in postsynaptic AMPA receptor expression or function but rather presynaptic alterations in $Cln3^{-/-}$ mice. In particular, the authors reported altered short-term plasticity under conditions of reduced extracellular Ca^{2+}, which may be associated with disturbed Ca^{2+} handling and sensing (55). Moreover, a reduced density of synaptic vesicles and decreased numbers of membrane adjacent synaptic vesicles in $Cln3^{-/-}$ mice were found in that study (55). In accordance with this, Grünewald *et al.* (56) found severely affected excitatory and inhibitory synaptic transmission, including the loss of GABAergic interneurons in the amygdala, hippocampus, and cerebellum of $Cln3^{-/-}$ mice. Cerebellar network activity depends critically on Kv4 channels and their fine-

tuning via the NCS protein KChIP3 (27, 57–60). In particular, long-term potentiation at the mossy fiber–granule cell synapse involves the modulation of postsynaptic Kv4 channels by shifting the voltage dependence of activation and inactivation (60). Moreover, cerebellar granule cell excitability in different subregions of the cerebellum is governed by the expression pattern of specific combinations of Kv4 and Ca^{2+} channels, thereby allowing input-specific processing of information via the NCS protein KChIP3 (58). KChIP3-mediated regulation of Kv4 channels also controls the excitability of cerebellar stellate cells, which provide inhibition of Purkinje cells (27). The Ca^{2+}-dependent regulation of A-type potassium channels determines the spike latency in stellate cells (59) and maintains inhibitory charge transfer to the Purkinje cells especially during extracellular Ca^{2+} fluctuations (57). All of these aspects of Ca^{2+}-dependent KChIP3-mediated modulation of Kv4 channels may be strongly impaired in JNCL, in which CLN3 loss of function leads to disturbed Ca^{2+} homeostasis. It remains to be seen whether and how altered somatodendritic A-type channel expression and function caused by loss of CLN3 function is causally involved in JNCL.

Experimental procedures

DNA plasmids and constructs

We used a human epitope-tagged Kv4.2 construct (C-terminal GFP tag: Kv4.2–GFP) (14, 61) cloned into a pcDNA3 expression vector, and the human KChIP3a splice variant (12) cloned into a pUC derivative (gift from Henry Jerng, Baylor College of Medicine, Houston, TX, USA). In addition we used WT CLN3 and JNCL-related mutants cloned into pcDNA3. The WT CLN3 clone produces a 438-amino acid multispanning transmembrane protein (Fig. S1). One mutant ($CLN3_{R334C}$) had a single amino acid substitution (cysteine for arginine) at position 334 (caused by a missense mutation in exon 13 of the *CLN3* gene in JNCL patients; NCL Mutation and Patient Database (RRID: SCR_018806)) (45). The other mutant (CLN3ΔC) showed a novel amino acid sequence beyond position 153 and a premature stop after position 181 (Fig. S1; caused by a 1.02-kb gene deletion and a resulting frameshift in the *CLN3* gene of JNCL patients). For the co-IP experiments, we cloned epitope-tagged KChIP3a and CLN3 constructs: a C-terminal Myc-tag (amino acids EQKLISEEDL) was attached to KChIP3a (KChIP3–Myc). KChIP3a was amplified by PCR using primers KChIP3-F (5′-CACCATGCAGCCGGCTAAGGAAGTGAC-3′) and KChIP3-R (5′-CTACAGATCCTCTTCTGAGATGAGTTTTTGTTCGATGACATTCTCAAACAGC-3′) and cloned into the expression vector pcDNA3.1D/V5-His-TOPO (Invitrogen). To generate a GFP–CLN3 fusion protein human CLN3 cDNA was amplified by PCR using primers CLN3-F (5′-GCAGATCTGGAGGCTGTGCAGGCTCGCGG-3′) and CLN3-R (5′-GCAGATCTTCAGGAGAGCTGGCAGAGGAAGTCATGC-3′). The resulting PCR products were digested with BglII and cloned into corresponding sites of the expression vector pEGFP-C1 (BD Biosciences). To generate an N-terminally HA-tagged (amino acids YPYDVPDYA) CLN3 construct (HA–CLN3), the human CLN3 cDNA was amplified by PCR using primers CLN3-F (5′-CACCATGGCGTACCCATACGACGTCCCAGACTACGCTGGAGGCTGTGCAGGCTCGCGG-3′) and CLN3-R (5′-CGGGATCCCGTCAGGAGAGCTGGC-3′), and the amplified PCR products were cloned into the expression vector pcDNA3.1D V5-His-TOPO. Except for the co-IP experiments, epitope-tagged Kv4.2 and the KChIP3a splice variant will be referred to as Kv4.2 and KChIP3, respectively, below.

Cell lines and transfection

Proteins were expressed in HEK 293 cells, grown under standard conditions (37 °C, 5% CO_2) in Dulbecco's minimal essential medium/NUT Mix F12 (Invitrogen) supplemented with heat-inactivated fetal bovine serum (10%, Seromed Biochrom) and penicillin–streptomycin–glutamine (1%, Invitrogen). One day after plating (8×10^5 cells/60-mm dish for co-IP, $1–4 \times 10^4$ cells/35-mm dish for electrophysiology), the cells were transiently transfected with expression vectors using Lipofectamine (Gibco; μg cDNA per dish for co-IP: GFP 2, Kv4.2–GFP 2, GFP–CLN3 2, KChIP3–Myc 2, CLN3 1, HA–CLN3 2; μg of cDNA per dish for electrophysiology: Kv4.2 0.1, KChIP3 0.25, CLN3 2.5). For some electrophysiology experiments, a stable Kv4.2-expressing cell line was used (62), and KChIP3 and CLN3 cDNAs were transiently co-transfected at different amounts (μg cDNA per dish: KChIP3 0.25, CLN3 2.5; *i.e.* 1:10; or KChIP3 0.1, CLN3 2; *i.e.* 1:20). Empty pcDNA3.1 vector was co-transfected to adjust absolute cDNA amounts if necessary, and EGFP or ds-Red (0.5 μg cDNA per dish) were co-transfected as marker plasmids to identify successfully transfected cells by fluorescence microscopy for electrophysiology experiments.

Antibodies

Primary antibodies were polyclonal rabbit anti–glyceraldehyde-3-phosphate dehydrogenase (Santa Cruz Biotechnology), monoclonal mouse anti-GFP, monoclonal rat anti-HA (Roche), monoclonal mouse anti-Myc (Cell Signalling), and monoclonal mouse anti–α-tubulin (Sigma–Aldrich). Secondary goat anti-mouse, goat anti-rabbit, and rabbit anti-rat antibodies coupled to horseradish peroxidase were from Dianova (Hamburg, Germany).

Co-IP and Western blotting analysis

24 h after the start of transfection, the growth medium was aspirated, and the cells were washed with ice-cold PBS, scraped in 1.5 ml of ice-cold PBS, and centrifuged for 5 min at $1,000 \times g$ at 4 °C. The cell pellets were lysed in 100 μl of ice-cold lysis buffer (10 mM Tris-Cl, pH 7.5, 0.5% Nonidet P-40, 150 mM NaCl, 0.5 mM EDTA, protease inhibitors) and placed on ice for 30 min. Where indicated, lysis, dilution and wash buffers lacking EDTA were supplemented with Ca^{2+} at a final concentration of 15 nM and 50 μM, respectively. The cell lysates were centrifuged at $20,000 \times g$ for 15 min at 4 °C, and the supernatants transferred to a new tube. Then 150 μl of ice-cold dilution buffer (10 mM Tris-Cl, pH 7.5, 150 mM NaCl, 0.5 mM EDTA, protease inhibitors) was added to the lysate, and aliquots (input) were removed for Western blotting analysis. Based on calculations with the program WEBMAXC extended (RRID: SCR_018807), the free Ca^{2+} concentration in the dilution

buffer was adjusted to 0 nM (nominal Ca^{2+}-free), 15 nM, or 50 μM. The lysates were mixed with 25 µl of GFP–TRAP bead slurry (ChromoTek) and incubated for 2 h at 4 °C on a rotating wheel. After centrifugation at 2,500 × *g*, the supernatants were removed, and the beads were washed three times with 500 µl of ice-cold dilution buffer. GFP–TRAP beads were resuspended in 75 µl of 2× SDS sample buffer and boiled for 10 min at 95 °C. Aliquots of the input and the eluates were separated by SDS-PAGE and analyzed by Myc immunoblotting. Immunoreactive bands were visualized by enhanced chemiluminescence detection using a molecular imager (model ChemiDoc XRS system, Bio-Rad).

Electrophysiological recordings

All recordings were done at room temperature (~22 °C) in the whole-cell configuration of the patch-clamp technique using an EPC9 amplifier and PULSE software (Heka Electronics). The cells were bathed in external solution containing 135 mM NaCl, 5 mM KCl, 2 mM $CaCl_2$, 2 mM $MgCl_2$, 5 mM HEPES, 10 mM sucrose, pH 7.4 (NaOH). Patch-pipettes were pulled from thin-walled borosilicate glass and filled with standard intracellular solution containing 125 mM KCl, 1 mM $CaCl_2$, 1 mM $MgCl_2$, 11 mM EGTA, 10 mM HEPES, 2 mM K_2-ATP, 2 mM GSH, pH 7.2 (KOH). The free Ca^{2+} concentration of this pipette solution was ~15 nM. Alternatively, a nominal Ca^{2+}-free pipette solution and one with 50 μM Ca^{2+} were used in some experiments as described previously (63) (EBMAXC extended). Pipette-to-bath resistances ranged between 2.5 and 3 MΩ, and series resistance compensation was between 80 and 90%. Currents were activated by voltage pulses to +40 mV from different prepulse voltages and with different interpulse intervals. In the absence of significant endogenous currents, leak subtraction was done based on a P/5 protocol. Subtraction of both leak and endogenous currents was done with a prepulse–inactivation–subtraction protocol (64).

Data analysis

Quantification of immunoreactive band intensities was performed using the software QuantityOne 4.5.0 (Bio-Rad). The current traces were analyzed with PulseFit (Heka Electronics), and the obtained data were further processed with Kaleidagraph (Synergy Software). Macroscopic current decay kinetics were described by the sum of three exponential functions (64), the kinetics of recovery from inactivation by a single-exponential function or by a double-exponential function with a weighted time constant. The voltage dependence of steady-state inactivation was described by a Boltzmann function of the form $I/I_{max} = 1/(1 + \exp(V - V_{1/2\ inact})/k)$, where V is the prepulse voltage, $V_{1/2\ inact}$ is the prepulse voltage that causes half-maximal inactivation, and k is the slope factor of the voltage dependence. Statistical analyses were done with Kaleidagraph and Prism (GraphPad Software). Comparison of band intensities for two groups and current densities for one group on d1 and d2 was done using unpaired Student's *t* test. Comparison of electrophysiological parameters for more than two groups on d2 was done using one-way analysis of variance (ANOVA) with Dunnett's post hoc testing.

Data availability

All data and statistical analyses are summarized in the supporting tables.

Acknowledgments—We thank Annett Hasse and Margrit Hölzel for cell line maintenance and Frank Stehr (NCL-Stiftung, Hamburg, Germany) and Thomas Braulke for discussion.

Author contributions—C. S. and S. S. data curation; C. S. and S. S. formal analysis; C. S. and S. S. investigation; C. S. and S. S. methodology; C. S., S. S., and R. B. writing-review and editing; R. B. conceptualization; R. B. funding acquisition; R. B. writing-original draft; R. B. project administration.

Funding and additional information—This work was supported by Grants BA 2055/4 and BA 2055/6 from the Deutsche Forschungsgemeinschaft (to R. B.).

Conflict of interest— The authors declare that they have no conflicts of interest with the contents of this article.

Abbreviations—The abbreviations used are: Kv channel, voltage-gated potassium channel; KChIP, Kv channel-interacting protein; DPP, dipeptidyl-aminopeptidase-related protein; DREAM, downstream regulatory element antagonist modulator; (J)NCL, (juvenile) neuronal ceroid lipofuscinosis; HEK, human embryonic kidney; IP, immunoprecipitation; IB, immunoblotting; d1 and d2, first and second day after transfection; NCS, neuronal calcium sensor; AMPA, α-amino-3-hydroxy-5-methyl-4-isoxazolepropionic acid; GST, glutathione *S*-transferase; ER, endoplasmic reticulum; HA, hemagglutinin; ANOVA, analysis of variance; CLN3, ceroid lipofuscinosis neuronal 3.

References

1. Hille, B. (2001) *Ion Channels of Excitable Membranes*, 3rd ed., Sinauer Associates, Inc., Sunderland, MA
2. Serôdio, P., Kentros, C., and Rudy, B. (1994) Identification of molecular components of A-type channels activating at subthreshold potentials. *J. Neurophysiol.* **72,** 1516–1529 CrossRef Medline
3. Hoffman, D. A., Magee, J. C., Colbert, C. M., and Johnston, D. (1997) K^+ channel regulation of signal propagation in dendrites of hippocampal pyramidal neurons. *Nature* **387,** 869–875 CrossRef Medline
4. Ramakers, G. M., and Storm, J. F. (2002) A postsynaptic transient K^+ current modulated by arachidonic acid regulates synaptic integration and threshold for LTP induction in hippocampal pyramidal cells. *Proc. Natl. Acad. Sci. U.S.A.* **99,** 10144–10149 CrossRef Medline
5. Bernard, C., Anderson, A., Becker, A., Poolos, N. P., Beck, H., and Johnston, D. (2004) Acquired dendritic channelopathy in temporal lobe epilepsy. *Science* **305,** 532–535 CrossRef Medline
6. Castro, P. A., Cooper, E. C., Lowenstein, D. H., and Baraban, S. C. (2001) Hippocampal heterotopia lack functional Kv4.2 potassium channels in the methylazoxymethanol model of cortical malformations and epilepsy. *J. Neurosci.* **21,** 6626–6634 CrossRef Medline
7. Francis, J., Jugloff, D. G., Mingo, N. S., Wallace, M. C., Jones, O. T., Burnham, W. M., and Eubanks, J. H. (1997) Kainic acid-induced generalized seizures alter the regional hippocampal expression of the rat Kv4.2 potassium channel gene. *Neurosci. Lett.* **232,** 91–94 CrossRef Medline
8. Lugo, J. N., Barnwell, L. F., Ren, Y., Lee, W. L., Johnston, L. D., Kim, R., Hrachovy, R. A., Sweatt, J. D., and Anderson, A. E. (2008) Altered

phosphorylation and localization of the A-type channel, Kv4.2 in status epilepticus. *J. Neurochem.* **106,** 1929–1940 CrossRef Medline
9. Monaghan, M. M., Menegola, M., Vacher, H., Rhodes, K. J., and Trimmer, J. S. (2008) Altered expression and localization of hippocampal A-type potassium channel subunits in the pilocarpine-induced model of temporal lobe epilepsy. *Neuroscience* **156,** 550–562 CrossRef Medline
10. Su, T., Cong, W. D., Long, Y. S., Luo, A. H., Sun, W. W., Deng, W. Y., and Liao, W. P. (2008) Altered expression of voltage-gated potassium channel 4.2 and voltage-gated potassium channel 4-interacting protein, and changes in intracellular calcium levels following lithium-pilocarpine-induced status epilepticus. *Neuroscience* **157,** 566–576 CrossRef Medline
11. Tsaur, M. L., Sheng, M., Lowenstein, D. H., Jan, Y. N., and Jan, L. Y. (1992) Differential expression of K^+ channel mRNAs in the rat brain and down-regulation in the hippocampus following seizures. *Neuron* **8,** 1055–1067 CrossRef Medline
12. An, W. F., Bowlby, M. R., Betty, M., Cao, J., Ling, H. P., Mendoza, G., Hinson, J. W., Mattsson, K. I., Strassle, B. W., Trimmer, J. S., and Rhodes, K. J. (2000) Modulation of A-type potassium channels by a family of calcium sensors. *Nature* **403,** 553–556 CrossRef Medline
13. Nadal, M. S., Ozaita, A., Amarillo, Y., Vega-Saenz de Miera, E., Ma, Y., Mo, W., Goldberg, E. M., Misumi, Y., Ikehara, Y., Neubert, T. A., and Rudy, B. (2003) The CD26-related dipeptidyl aminopeptidase-like protein DPPX is a critical component of neuronal A-type K^+ channels. *Neuron* **37,** 449–461 CrossRef Medline
14. Bähring, R., Dannenberg, J., Peters, H. C., Leicher, T., Pongs, O., and Isbrandt, D. (2001) Conserved Kv4 N-terminal domain critical for effects of Kv channel-interacting protein 2.2 on channel expression and gating. *J. Biol. Chem.* **276,** 23888–23894 CrossRef Medline
15. Shibata, R., Misonou, H., Campomanes, C. R., Anderson, A. E., Schrader, L. A., Doliveira, L. C., Carroll, K. I., Sweatt, J. D., Rhodes, K. J., and Trimmer, J. S. (2003) A fundamental role for KChIPs in determining the molecular properties and trafficking of Kv4.2 potassium channels. *J. Biol. Chem.* **278,** 36445–36454 CrossRef Medline
16. Zagha, E., Ozaita, A., Chang, S. Y., Nadal, M. S., Lin, U., Saganich, M. J., McCormack, T., Akinsanya, K. O., Qi, S. Y., and Rudy, B. (2005) DPP10 modulates Kv4-mediated A-type potassium channels. *J. Biol. Chem.* **280,** 18853–18861 CrossRef Medline
17. Beck, E. J., Bowlby, M., An, W. F., Rhodes, K. J., and Covarrubias, M. (2002) Remodelling inactivation gating of Kv4 channels by KChIP1, a small-molecular-weight calcium-binding protein. *J. Physiol.* **538,** 691–706 CrossRef Medline
18. Jerng, H. H., Qian, Y., and Pfaffinger, P. J. (2004) Modulation of Kv4.2 channel expression and gating by dipeptidyl peptidase 10 (DPP10). *Biophys. J.* **87,** 2380–2396 CrossRef Medline
19. Pruunsild, P., and Timmusk, T. (2005) Structure, alternative splicing, and expression of the human and mouse KCNIP gene family. *Genomics* **86,** 581–593 CrossRef Medline
20. Carrión, A. M., Link, W. A., Ledo, F., Mellström, B., and Naranjo, J. R. (1999) DREAM is a Ca^{2+}-regulated transcriptional repressor. *Nature* **398,** 80–84 CrossRef Medline
21. Buxbaum, J. D., Choi, E. K., Luo, Y., Lilliehook, C., Crowley, A. C., Merriam, D. E., and Wasco, W. (1998) Calsenilin: a calcium-binding protein that interacts with the presenilins and regulates the levels of a presenilin fragment. *Nat. Med.* **4,** 1177–1181 CrossRef Medline
22. Bähring, R. (2018) Kv channel-interacting proteins as neuronal and non-neuronal calcium sensors. *Channels* **12,** 187–200 CrossRef Medline
23. Chang, J. W., Choi, H., Kim, H. J., Jo, D. G., Jeon, Y. J., Noh, J. Y., Park, W. J., and Jung, Y. K. (2007) Neuronal vulnerability of CLN3 deletion to calcium-induced cytotoxicity is mediated by calsenilin. *Hum. Mol. Genet.* **16,** 317–326 CrossRef Medline
24. Consortium, T. I. B. D. (1995) Isolation of a novel gene underlying Batten disease, *CLN3. Cell* **82,** 949–957 CrossRef Medline
25. Mirza, M., Vainshtein, A., DiRonza, A., Chandrachud, U., Haslett, L. J., Palmieri, M., Storch, S., Groh, J., Dobzinski, N., Napolitano, G., Schmidtke, C., and Kerkovich, D. M. (2019) The CLN3 gene and protein: what we know. *Mol. Genet. Genomic Med.* **7,** e859 CrossRef Medline
26. Williams, R. E., and Mole, S. E. (2012) New nomenclature and classification scheme for the neuronal ceroid lipofuscinoses. *Neurology* **79,** 183–191 CrossRef Medline
27. Anderson, D., Mehaffey, W. H., Iftinca, M., Rehak, R., Engbers, J. D., Hameed, S., Zamponi, G. W., and Turner, R. W. (2010) Regulation of neuronal activity by Cav3–Kv4 channel signaling complexes. *Nat. Neurosci.* **13,** 333–337 CrossRef Medline
28. Shen, J., and Kelleher, R. J., 3rd (2007) The presenilin hypothesis of Alzheimer's disease: evidence for a loss-of-function pathogenic mechanism. *Proc. Natl. Acad. Sci. U.S.A.* **104,** 403–409 CrossRef Medline
29. Leissring, M. A., Yamasaki, T. R., Wasco, W., Buxbaum, J. D., Parker, I., and LaFerla, F. M. (2000) Calsenilin reverses presenilin-mediated enhancement of calcium signaling. *Proc. Natl. Acad. Sci. U.S.A.* **97,** 8590–8593 CrossRef Medline
30. Lilliehook, C., Chan, S., Choi, E. K., Zaidi, N. F., Wasco, W., Mattson, M. P., and Buxbaum, J. D. (2002) Calsenilin enhances apoptosis by altering endoplasmic reticulum calcium signaling. *Mol. Cell. Neurosci.* **19,** 552–559 CrossRef Medline
31. Jo, D. G., Jang, J., Kim, B. J., Lundkvist, J., and Jung, Y. K. (2005) Overexpression of calsenilin enhances γ-secretase activity. *Neurosci. Lett.* **378,** 59–64 CrossRef Medline
32. Jo, D. G., Chang, J. W., Hong, H. S., Mook-Jung, I., and Jung, Y. K. (2003) Contribution of presenilin/γ-secretase to calsenilin-mediated apoptosis. *Biochem. Biophys. Res. Commun.* **305,** 62–66 CrossRef Medline
33. Menegola, M., and Trimmer, J. S. (2006) Unanticipated region- and cell-specific downregulation of individual KChIP auxiliary subunit isotypes in Kv4.2 knock-out mouse brain. *J. Neurosci.* **26,** 12137–12142 CrossRef Medline
34. Norris, A. J., Foeger, N. C., and Nerbonne, J. M. (2010) Interdependent roles for accessory KChIP2, KChIP3, and KChIP4 subunits in the generation of Kv4-encoded I_A channels in cortical pyramidal neurons. *J. Neurosci.* **30,** 13644–13655 CrossRef Medline
35. Getty, A. L., and Pearce, D. A. (2011) Interactions of the proteins of neuronal ceroid lipofuscinosis: clues to function. *Cell. Mol. Life Sci.* **68,** 453–474 CrossRef Medline
36. Phillips, S. N., Benedict, J. W., Weimer, J. M., and Pearce, D. A. (2005) CLN3, the protein associated with Batten disease: structure, function and localization. *J. Neurosci. Res.* **79,** 573–583 CrossRef Medline
37. Murphy, J. G., and Hoffman, D. A. (2019) A polybasic motif in alternatively spliced KChIP2 isoforms prevents Ca^{2+} regulation of Kv4 channels. *J. Biol. Chem.* **294,** 3683–3695 CrossRef Medline
38. Uusi-Rauva, K., Luiro, K., Tanhuanpää, K., Kopra, O., Martín-Vasallo, P., Kyttälä, A., and Jalanko, A. (2008) Novel interactions of CLN3 protein link Batten disease to dysregulation of fodrin–Na^+,K^+ ATPase complex. *Exp. Cell Res.* **314,** 2895–2905 CrossRef Medline
39. Kovács, A. D., and Pearce, D. A. (2015) Finding the most appropriate mouse model of juvenile CLN3 (Batten) disease for therapeutic studies: the importance of genetic background and gender. *Dis. Model. Mech.* **8,** 351–361 CrossRef Medline
40. Shacka, J. J. (2012) Mouse models of neuronal ceroid lipofuscinoses: useful pre-clinical tools to delineate disease pathophysiology and validate therapeutics. *Brain. Res. Bull.* **88,** 43–57 CrossRef Medline
41. Palmer, D. N. (2015) The relevance of the storage of subunit c of ATP synthase in different forms and models of Batten disease (NCLs). *Biochim. Biophys. Acta* **1852,** 2287–2291 CrossRef Medline
42. Cao, Y., Espinola, J. A., Fossale, E., Massey, A. C., Cuervo, A. M., MacDonald, M. E., and Cotman, S. L. (2006) Autophagy is disrupted in a knock-in mouse model of juvenile neuronal ceroid lipofuscinosis. *J. Biol. Chem.* **281,** 20483–20493 CrossRef Medline
43. Chandrachud, U., Walker, M. W., Simas, A. M., Heetveld, S., Petcherski, A., Klein, M., Oh, H., Wolf, P., Zhao, W. N., Norton, S., Haggarty, S. J., Lloyd-Evans, E., and Cotman, S. L. (2015) Unbiased cell-based screening in a neuronal cell model of Batten disease highlights an interaction between Ca^{2+} homeostasis, autophagy, and CLN3 protein function. *J. Biol. Chem.* **290,** 14361–14380 CrossRef Medline
44. Lopez-Hurtado, A., Peraza, D. A., Cercos, P., Lagartera, L., Gonzalez, P., Dopazo, X. M., Herranz, R., Gonzalez, T., Martin-Martinez, M., Mellstrom, B., Naranjo, J. R., Valenzuela, C., and Gutierrez-Rodriguez, M.

(2019) Targeting the neuronal calcium sensor DREAM with small-molecules for Huntington's disease treatment. *Sci. Rep.* **9,** 7260 CrossRef Medline

45. Munroe, P. B., Mitchison, H. M., O'Rawe, A. M., Anderson, J. W., Boustany, R. M., Lerner, T. J., Taschner, P. E., de Vos, N., Breuning, M. H., Gardiner, R. M., and Mole, S. E. (1997) Spectrum of mutations in the Batten disease gene, CLN3. *Am. J. Hum. Genet.* **61,** 310–316 CrossRef Medline
46. Haskell, R. E., Carr, C. J., Pearce, D. A., Bennett, M. J., and Davidson, B. L. (2000) Batten disease: evaluation of CLN3 mutations on protein localization and function. *Hum. Mol. Genet.* **9,** 735–744 CrossRef Medline
47. Järvelä, I., Lehtovirta, M., Tikkanen, R., Kyttälä, A., and Jalanko, A. (1999) Defective intracellular transport of CLN3 is the molecular basis of Batten disease (JNCL). *Hum. Mol. Genet.* **8,** 1091–1098 CrossRef Medline
48. Chan, C. H., Mitchison, H. M., and Pearce, D. A. (2008) Transcript and *in silico* analysis of CLN3 in juvenile neuronal ceroid lipofuscinosis and associated mouse models. *Hum. Mol. Genet.* **17,** 3332–3339 CrossRef Medline
49. Kitzmüller, C., Haines, R. L., Codlin, S., Cutler, D. F., and Mole, S. E. (2008) A function retained by the common mutant CLN3 protein is responsible for the late onset of juvenile neuronal ceroid lipofuscinosis. *Hum. Mol. Genet.* **17,** 303–312 CrossRef Medline
50. Autti, T., Raininko, R., Vanhanen, S. L., and Santavuori, P. (1996) MRI of neuronal ceroid lipofuscinosis: I. Cranial MRI of 30 patients with juvenile neuronal ceroid lipofuscinosis. *Neuroradiology* **38,** 476–482 CrossRef Medline
51. Nardocci, N., Verga, M. L., Binelli, S., Zorzi, G., Angelini, L., and Bugiani, O. (1995) Neuronal ceroid-lipofuscinosis: a clinical and morphological study of 19 patients. *Am. J. Med. Genet.* **57,** 137–141 CrossRef Medline
52. Raininko, R., Santavuori, P., Heiskala, H., Sainio, K., and Palo, J. (1990) CT findings in neuronal ceroid lipofuscinoses. *Neuropediatrics* **21,** 95–101 CrossRef Medline
53. Finn, R., Kovács, A. D., and Pearce, D. A. (2011) Altered sensitivity of cerebellar granule cells to glutamate receptor overactivation in the *Cln3*$^{\Delta ex7/8}$–knock-in mouse model of juvenile neuronal ceroid lipofuscinosis. *Neurochem. Int.* **58,** 648–655 CrossRef Medline
54. Kovács, A. D., Weimer, J. M., and Pearce, D. A. (2006) Selectively increased sensitivity of cerebellar granule cells to AMPA receptor-mediated excitotoxicity in a mouse model of Batten disease. *Neurobiol. Dis.* **22,** 575–585 CrossRef Medline
55. Studniarczyk, D., Needham, E. L., Mitchison, H. M., Farrant, M., and Cull-Candy, S. G. (2018) Altered cerebellar short-term plasticity but no change in postsynaptic AMPA-type glutamate receptors in a mouse model of juvenile Batten disease. *eNeuro* **5,** ENEURO.0387-17.2018 CrossRef Medline
56. Grünewald, B., Lange, M. D., Werner, C., O'Leary, A., Weishaupt, A., Popp, S., Pearce, D. A., Wiendl, H., Reif, A., Pape, H. C., Toyka, K. V., Sommer, C., and Geis, C. (2017) Defective synaptic transmission causes disease signs in a mouse model of juvenile neuronal ceroid lipofuscinosis. *eLife* **6,** e28685 CrossRef Medline
57. Anderson, D., Engbers, J. D., Heath, N. C., Bartoletti, T. M., Mehaffey, W. H., Zamponi, G. W., and Turner, R. W. (2013) The Cav3-Kv4 complex acts as a calcium sensor to maintain inhibitory charge transfer during extracellular calcium fluctuations. *J. Neurosci.* **33,** 7811–7824 CrossRef Medline
58. Heath, N. C., Rizwan, A. P., Engbers, J. D., Anderson, D., Zamponi, G. W., and Turner, R. W. (2014) The expression pattern of a Cav3-Kv4 complex differentially regulates spike output in cerebellar granule cells. *J. Neurosci.* **34,** 8800–8812 CrossRef Medline
59. Molineux, M. L., Fernandez, F. R., Mehaffey, W. H., and Turner, R. W. (2005) A-type and T-type currents interact to produce a novel spike latency-voltage relationship in cerebellar stellate cells. *J. Neurosci.* **25,** 10863–10873 CrossRef Medline
60. Rizwan, A. P., Zhan, X., Zamponi, G. W., and Turner, R. W. (2016) Long-term potentiation at the mossy fiber-granule cell relay invokes postsynaptic second-messenger regulation of Kv4 channels. *J. Neurosci.* **36,** 11196–11207 CrossRef Medline
61. Prechtel, H., Hartmann, S., Minge, D., and Bähring, R. (2018) Somatodendritic surface expression of epitope-tagged and KChIP binding-deficient Kv4.2 channels in hippocampal neurons. *PLoS One* **13,** e0191911 CrossRef Medline
62. Hartmann, S. (2007) Funktionelle Interaktion des Kv4.2-Proteins mit akzessorischen Untereinheiten - Rolle für die somatodendritische A-Typ-Kanal-Expression in hippokampalen Neuronen von Maus (Mus musculus, Linné, 1758) und Ratte (Rattus norvegicus, Berkenhout, 1769), Ph.D. Thesis, University of Hamburg, Hamburg, Germany
63. Groen, C., and Bähring, R. (2017) Modulation of human Kv4.3/KChIP2 channel inactivation kinetics by cytoplasmic Ca^{2+}. *Pflügers. Arch.* **469,** 1457–1470 CrossRef Medline
64. Bähring, R., Boland, L. M., Varghese, A., Gebauer, M., and Pongs, O. (2001) Kinetic analysis of open- and closed-state inactivation transitions in human Kv4.2 A-type potassium channels. *J. Physiol.* **535,** 65–81 CrossRef Medline